The Journal of Neuroscience

http://jneurosci.msubmit.net

JN-RM-1350-16R3

Phase-dependent interactions in visual cortex to combinations of first- and second-order stimuli

Curtis Baker Jr, McGill University
Claire Hutchinson, University of Leicester
Timothy Ledgeway, The University of Nottingham

Commercial Interest:

Phase-dependent interactions in visual cortex to combinations of first- and second-order stimuli

Abbreviated title: Phase-dependent second-order responses

Claire V. Hutchinson[1], Timothy Ledgeway[2], & Curtis L. Baker, Jr. [3*]

[1]College of Medicine, Biological Sciences and Psychology, University of Leicester, Leicester, United Kingdom, LE1 9HN

[2]School of Psychology, University of Nottingham, Nottingham, United Kingdom, NG7 2RD

[3]McGill Vision Research Unit, MUHC Research Institute, Department of Ophthalmology, McGill University, Montreal, QC, Canada H3A 1A1

***Correspondence should be addressed to:**

Curtis L. Baker Jr

McGill Vision Research

MUHC Research Institute

1650 Cedar Ave, Room L11.112

Montreal, Quebec, Canada, H3G 1A4

Tel: +1-514-934-1934 ext.34819

Fax: +1-514-934-8216

Email: curtis.baker@mcgill.ca

Number of pages: 35

Number of figures: 8

Number of words for Abstract: 230

Number of words for Introduction: 467

Number of words for Discussion: 1497

Conflict of interest: none

Acknowledgements:

This research was supported by CIHR Operating Grants (MOP-119498, MOP-9685) to C.B. C.V.H was supported, in part, by a Human Frontier Science Program Organization Short Term Fellowship. The authors would like to thank Lynda Domazet, Guangxing Li, and Vargha Talebi for assistance with some of the experiments. The authors declare no competing financial interests.

1

Abstract

A fundamental task of the visual system is to extract figure-ground boundaries between objects, which are often defined not only by differences in luminance but also by "second-order" contrast or texture differences. Responses of cortical neurons to both first- and second-order patterns have been previously studied extensively, but only for responses to either type of stimulus in isolation. Here we examined responses of visual cortex neurons to the spatial relationship between superimposed periodic luminance modulation (LM) and contrast modulation (CM) stimuli, whose contrasts were adjusted to give equated responses when presented alone. Extracellular single unit recordings were made in area 18 of the cat, whose neurons show very similar responses to CM and LM stimuli as those in primate area V2 (Li et al, 2014). Most neurons showed a significant dependence on the relative phase of the combined LM and CM patterns, with a clear overall optimal response when they were approximately phase-aligned. The degree of this phase preference, and the contributions of suppressive and/or facilitatory interactions, varied considerably from one neuron to another. Such phase-dependent and phase-invariant responses were evident in both simple- and complex-type cells. These results place important constraints on any future model of the underlying neural circuitry for second-order responses. The diversity in the degree of phase dependence between LM and CM stimuli that we observe could help disambiguate different kinds of boundaries in natural scenes.

Significance

Many visual cortex neurons exhibit orientation-selective responses to boundaries defined by differences either in luminance or in texture contrast. Previous studies have examined responses to either type of boundary in isolation, but here we systematically measure responses of cortical neurons to the spatial relationship between superimposed periodic luminance-modulated (LM) and contrast-modulated (CM) stimuli whose contrasts are adjusted to give equated responses. We demonstrate that neuronal responses to these compound stimuli are highly dependent on the relative phase between the LM and CM components. Diversity in the degree of such phase dependence could help disambiguate different kinds of boundaries in natural scenes, for example those arising from surface reflectance changes or from illumination gradients such as shading or shadows.

Introduction

Natural scenes contain a multiplicity of complex features that provide important information concerning object position, surface structure, boundaries and contours, spatial scale, motion and relative distance. The visual system uses these cues to detect and identify objects in a scene by segregating them from their background. An object may be delineated from its background by intensive "first-order" properties, e.g. variations in luminance or color within different regions of the image, or by more complex "second-order" attributes in which areas are differentiated by cues such as contrast, texture, relative motion and binocular disparity. In natural images, there is a highly structured spatial relationship between occurrences of first- and second-order information (Schofield, 2000; Johnson & Baker, 2004). Human psychophysical studies show that combined first- and second-order cues improve texture segmentation (Smith & Scott-Samuel, 1998; Johnson et al, 2007), and could potentially be used to help resolve ambiguities in first-order information, for example to distinguish surface reflectance vs. illumination effects (Schofield et al, 2006, 2010; Sun & Schofield, 2011).

Neurons responsive to both first- and second-order stimuli are evident in many visual cortical areas (V1, V2, V5/MT) of the monkey (Albright, 1992; Chaudhuri & Albright, 1997; Li et al, 2014; but see El-Shamayleh & Movshon, 2011) and areas 17 and 18 of the cat (Zhou & Baker, 1994; Tanaka & Ohzawa, 2006; Rosenberg & Issa, 2011). Many of these demonstrate form-cue invariance to first- and second-order motion patterns, in that they respond to either kind of stimulus with consistent direction-selectivity and preferred orientation (Albright, 1992; Geesaman & Anderson, 1996; Mareschal & Baker, 1999; Li et al, 2014). Human fMRI also reveals orientation- or direction-selective responses to first- and second-order stimuli in

many extrastriate cortical areas as well as primary visual cortex (Nishida et al, 2003; Seiffert et al, 2003; Larsson et al, 2006; Hallum et al, 2011).

In natural images, first- and second-order information often occur at coincident locations (Johnson & Baker, 2004), for example at occlusion boundaries. Therefore it is important to understand how these two types of information are combined in visual cortex. However previous neurophysiological studies have only examined neuronal responses to first- or second-order stimuli in isolation. Here we systematically measure responses of cortical neurons to the spatial relationship between superimposed periodic luminance-modulated (LM) and second-order contrast-modulated (CM) stimuli whose contrasts are adjusted to give equated responses. These recordings are done in area 18 of the cat, whose neurons show CM and LM responses largely similar to those in macaque area V2 (Li et al, 2014). We find that many of the neurons exhibit responses to compound stimuli that are highly dependent on the relative phase between the LM and CM components, with differing degrees of suppressive and/or facilitatory interactions in different neurons. Such phase-dependent and phase-invariant responses are evident in both simple- and complex-type cells.

Materials and methods

Animal Preparation and Maintenance

Initial anesthesia of adult cats of either sex was induced by isoflourane/oxygen (3-5%) inhalation, followed by intravenous cannulation and bolus I.V. delivery of thiopentone sodium (8 mg/kg) or propofol (5 mg/kg), atropine sulphate (0.05 mg/kg) and dexamethasone (0.2 mg/kg). The corneas were protected during surgery with topical carboxymethylcellulose

(1%). Surgical anesthesia was maintained with supplemental doses of thiopentone as required, or with propofol (6 mg/kg/hr), and all surgical wounds were infused with bupivacaine (0.25%). A secure airway was established by tracheal cannulation or intubation. A craniotomy (H-C A3/L4) provided access to cortical area 18 (Tusa et al, 1979) using glass-coated platinum-iridium or parylene-coated tungsten microelectrodes (Frederick Haer). The cortical surface was protected with 2% agarose (Sigma, Type 1-A) and petroleum jelly.

After completion of surgery, animals were paralyzed with an intravenous bolus injection of gallamine triethodide (10mg/kg), followed by infusion (10 mg/kg/hr). Anesthesia was maintained with sodium pentobarbital (1.0 mg/kg/hr) in earlier experiments, or with fentenyl (9 mcg/kg bolus, then 26 mcg/kg/hr) and propofol (5 mg/kg-hr) in later experiments, supplemented with oxygen/nitrous oxide (70:30) and dextrose-saline (2ml/hr). Expired CO_2, blood O_2, heart rate, electroencephalogram, and temperature were monitored throughout the experiment and maintained at appropriate levels. Corneal protection was provided by neutral contact lenses, and emmetropia at a distance of 57 cm was provided by spectacle lenses selected with slit retinoscopy, and artificial pupils (2.5 mm). All animal procedures were approved by the McGill University Animal Care Committee and are in accordance with the guidelines set out by the Canadian Council on Animal Care.

Visual Stimuli

Visual stimuli were produced on a Macintosh computer (MacPro 4,1, MacOS 10.6.8, 2.66 Ghz/4 core, 6 Gb, NVIDIA GeForce GT120) using custom software written in Matlab (The Mathworks) with the Psychophysics Toolbox (Brainard, 1997; Pelli, 1997; Kleiner et al, 2007). Stimulus patterns were displayed on a CRT monitor (NEC FP1350, 20”, 640x480 pixels, 75 Hz, 36 cd/m^2, bit depth 8), placed at a viewing distance of 57 cm. The monitor’s

gamma nonlinearity was measured with a photometer (United Detector Technology) and corrected with an inverse lookup table.

Three types of stimulus patterns were employed: first-order luminance-modulated (LM) gratings, second-order contrast-modulated (CM) envelopes, and a compound of the two (LM + CM). In each case, these were zero-balanced patterns of contrast against a mean luminance background, L_0.

Luminance gratings were spatially one-dimensional sinusoidal modulations (Fig. 1*A*,*B*):

$$L(x, y, t) = L_0\{1 + C_L \sin[2\pi(\omega_s(x \cos \theta + y \sin \theta) - \omega_t t)]\}, \quad (1)$$

where C_L = Michelson contrast of luminance modulation, ω_s = spatial frequency, θ = orientation, and ω_t = temporal frequency. The second-order stimuli ("contrast envelopes" - Fig. 1*C*,*D*) were spatially one-dimensional sinusoidal modulations of the contrast of a high-spatial frequency carrier grating:

$$L(x, y, t) = L_0\{1 + Carr(x, y)\,[1 + Env(x, y, t)] / 2\}, \quad (2)$$

The carrier grating was a high spatial frequency, stationary sine wave grating:

$$Carr(x, y) = C_c \sin[2\pi\,\omega_c(x \cos \theta_c + y \sin \theta_c)], \quad (3)$$

where C_c = carrier contrast, ω_c = carrier spatial frequency, and θ_c = carrier orientation. The carrier was multiplied by an envelope pattern, consisting of a low spatial frequency, drifting sine wave grating:

$$Env(x, y, t) = C_E \sin[2\pi (\omega_x x \cos\theta + y \sin\theta) - \omega_t t) + \phi], \quad (4)$$

where C_E = envelope contrast, ω_s and ω_t = envelope spatial and temporal frequency, and θ = envelope orientation. The compound stimuli were superpositions of the LM and CM patterns:

$$L(x, y, t) = L_0\{\{1 + Carr(x, y)\,[1 + Env(x, y, t)]\,/\,2\} + \{C_L \sin[2\pi (\omega_x x \cos\theta + y \sin\theta) - \omega_t t)]\}\}, \quad (5)$$

Note that these three stimuli have identical envelope orientation (θ) and spatial and temporal frequencies (ω_s, ω_t), but can have varying values of relative spatial phase (ϕ) — examples of single frames and 1-d profiles are shown in Figures 1*E,G* and 1*F,H* (ϕ = 0 and ϕ = 180 deg, respectively). LM and CM stimuli were considered to be "in-phase" (0 degrees) when the high and low luminance bars of the grating were centered on the high and low contrast bars of the envelope, and "anti-phase" (180 degrees) in the opposite case - this definition was determined *a priori*.

Stimulus patterns were presented within a cosine-tapered circular aperture, against a uniform background at the mean luminance of the pattern. The same mean luminance was also maintained during intervals between stimuli, and presented as blank conditions for measurement of spontaneous activity.

Electrophysiology

The microelectrode was advanced with a stepping-motor microdrive (M. Walsh Electronics, West Covina, CA). Single units were isolated with a window discriminator (Frederick Haer) and isolation was monitored on a delay-triggered oscilloscope. Manually controlled bar-shaped stimuli were used to approximately map the receptive field and determine ocular dominance. The display screen was centered on the receptive field and subsequent stimuli were delivered only to the neuron's dominant eye. Spike times were recorded with 0.1 msec resolution (ITC-18, Instrutech), and their temporal registration with the stimulus was established with reference to an optical sensor (T2L12S, TAOS, Texas) placed over a corner of the display containing stimulus timing information. Within an experimental run, different stimulus conditions were presented for 0.5-1.0 sec in randomly interleaved order (0.5 sec for LM gratings, 1.0 sec for CM or LM + CM stimuli), with 5-20 repetitions of each stimulus. Poststimulus time histograms and plots of average spike frequency as functions of varied stimulus parameters were displayed on-line. Spike times and stimulus information were recorded to hard disk files for subsequent detailed analysis.

Each neuron was quantitatively characterized with conventional tuning-curve measurements using first-order grating patterns to establish its optimal orientation, spatial/temporal frequency, simple/complex classification, and location and size of its receptive field. Each neuron was assessed for responsiveness to second-order stimuli using procedures like those employed previously (e.g., Mareschal & Baker, 1999; Tanaka & Ohzawa, 2006): contrast envelope stimuli were presented, using envelope parameters (orientation, spatial/temporal frequency) which were optimal for first-order stimuli, and a series of relatively high carrier spatial frequencies were tested (typically ~ 0.5 to 3.0 cpd). A neuron was considered

188 envelope-responsive if the data exhibited a bandpass tuned response to the spatial frequency
189 of the carrier, which was clearly distinct from its response to luminance gratings, such that
190 the contrast envelope response clearly could not be mediated by the same mechanism
191 underlying the response to first-order gratings. Then using this optimal carrier spatial
192 frequency, the response to a series of carrier orientations was systematically tested to further
193 optimize the response. All subsequent tests employed these individually optimized
194 parameters for contrast envelopes, and first-order luminance gratings were used with
195 parameters matched to those of the second-order envelopes.
196
197 Following these preliminary measurements, subsequent experiments were performed on
198 envelope-responsive neurons. Contrast response functions (Ledgeway et al, 2005) were
199 measured for both first-order (luminance grating) and second-order (contrast envelope)
200 stimuli, using identical values of envelope orientation and spatial/temporal frequency. From
201 these data, contrast values for the two stimuli were selected that would produce
202 approximately equated responses. Because neurons are typically more responsive to LM than
203 to CM patterns, we chose a high CM envelope contrast (typically 100%) and matched the
204 spike frequency with an equivalent LM contrast. Unless otherwise noted these values were
205 used for the compound (LM + CM) stimuli which were presented at a series of values of
206 relative spatial phase.
207
208 Quantitative measurements for this study were obtained from 76 neurons in nine animals.
209 Note that this work was carried out in conjunction with other studies on the same animals,
210 being conducted concurrently. Of these neurons, 28 were significantly envelope-responsive
211 and their isolation was maintained sufficiently long (ca 2 hours) to obtain all the preliminary

measurements and the contrast-response and phase-interaction datasets to qualify for inclusion in the study.

Data Analysis

Spike times were collected into poststimulus time histograms (bin width 10 msec), and plots of time-averaged spike frequency as functions of varied parameters were constructed. Neurons were classified as simple or complex type based on the ratio of response at the first harmonic of stimulus temporal frequency to the average firing rate (Skottun et al, 1991). Optimal parameters for descriptive mathematical functions (see below) were estimated using curve-fitting functionality of Kaleidagraph (Synergy Software) or Matlab (The Mathworks).

Results

Contrast response functions

Neurons were markedly less responsive to CM than to LM stimuli, consistent with previous studies (Ledgeway et al, 2005). To maximize the opportunity to detect interactions between the two stimuli, and ensure that the response would not be dominated by the LM stimulus, we amplitude-equated ('matched') the two stimulus types in terms of each neuron's responsiveness. This was achieved by measuring contrast response functions (CRFs) for each stimulus type, using optimized stimulus parameters as outlined above. Note that for each neuron the orientation, spatial frequency, temporal frequency and direction of motion of the modulation waveforms were identical for LM and CM, and in the case of CM the optimal carrier was also used. Based on these measurements we selected values of grating and envelope contrast that elicited an approximately equivalent response (Fig. 2*A,B*, green

dashed lines). A CM carrier contrast of 70% was used throughout to ensure that the sum of carrier contrast for CM and luminance contrast for LM would be physically realizable, i.e. not exceeding 100%.

Phase-dependent responses

LM and CM stimuli were superimposed, at their response-matched amplitudes, and responses (average spikes/sec) were recorded as a function of their relative spatial phase offset. In the example of a complex-type cell shown in Figure 2*C*, the response was markedly dependent on the relative spatial phase difference between LM and CM stimuli, with a peak response at a relative spatial phase somewhat greater than zero (close to phase-alignment, Fig. 1*C*). As the spatial phase offset between the two stimuli increased, responses became less vigorous, producing the weakest responses when LM and CM stimuli were close to anti-phase (180 deg, Fig. 1*F*).

To quantify the magnitude of spatial phase dependence of a neuron's responses, the measured spontaneous activity was subtracted, and the response R as a function of relative spatial phase ϕ was fit with a descriptive function:

$$R = a\,[0.5\,\langle 1 + \cos(\phi - \phi_{max})\rangle]^{0.5} + R_{min}, \qquad (6)$$

where ϕ is relative spatial phase between the stimuli, R_{min} is the minimum response (spikes/sec), a is a scaling factor, $\phi_{\max}$ is the spatial phase producing maximum response ($R_{max} = R_{min} + a$). This function corresponds to linear vector summation between two sinusoids of equivalent amplitude. R_{max} would only equal R_{min} if there were no vector summation (i.e. if the summation process was phase-invariant). An example of such a curve-

fit is shown by the blue contour in Figure 2*C* - for illustration, the spontaneous rate has been added back onto the fitted function values, to compare to the data points on the plots that also include the spontaneous rate.

To assess the degree of anisotropy in a neuron's response vs. the relative spatial phase, a phase-dependency index (PDI) was calculated as:

$$PDI = (R_{max} - R_{min}) / (R_{max} + R_{min}), \qquad (7)$$

where R_{max} and R_{min} are the maximal and minimal spontaneous-subtracted responses, respectively. This PDI value lies between zero, indicating no phase-dependent interaction (i.e. spike frequency remained relatively constant irrespective of the relative spatial phase between LM and CM), and unity, indicating a pronounced interaction (highest degree of anisotropy, with a well-defined null phase having zero response).

Six additional examples of such relative-phase responses are shown in Figure 3.
In the majority of cases exhibiting a marked phase interaction, maximal responses corresponded to a spatial phase offset close to 0 deg (in-phase). However, some neurons responded maximally at other relative spatial phase offsets (e.g. Fig. 3*E*). Minimal responses typically occurred around 180 deg relative to the phase offset that produced the maximal response and corresponded to either a distinct ‘null’ or to a general ‘flattening’ of responses at a number of phase offsets around anti-phase. However the responses of some neurons showed little or no phase dependency (e.g. the complex cell in Fig. 3*D*) and were largely invariant irrespective of the phase-relationship between the two superimposed visual stimuli.

For cells with low PDI, it is possible that the estimated ϕ_{max} could depend heavily on the initial value chosen for the curve fitting procedure. To address this concern, we re-ran the curve fitting for every neuron using a series of initial ϕ_{max} values. For this we used a least squares simplex (Nelder-Mead) method to fit Equation 6 repeatedly to each neuron's spontaneous-subtracted data, and systematically varied the initial ϕ_{max} estimate from 0 to 360 deg in steps of 1 deg. The initial estimates for the other curve-fit parameters were jittered by ±50% on each pass. We then found the set of best-fitting parameters that gave the highest goodness-of-fit (R^2) overall for each cell. Thus we are confident that the tendency for a ϕ_{max} close to 0 deg is not an artifact of initial conditions in the curve fitting procedure.

A scatterplot of PDI values and ϕ_{max} (deg) for each neuron in our sample (N = 28) is shown in Figure 4. Different neurons displayed a wide range of responses to the combined LM and CM patterns, with many examples exhibiting a 'peak' with maximal response at one particular spatial phase, and therefore having a PDI substantially greater than zero. A paired-samples t-test confirmed maximal and minimal responses were significantly different (t = 5.829; df = 27; $p < 0.0001$) across the sample population, demonstrating the existence of phase-dependent interactions between LM and CM responses. Irrespective of their PDI value, neurons typically produced their maximal responses at spatial phase offsets (ϕ_{max}) close to 0 deg. This was true of both simple (circles) and complex cells (triangles) (Fig. 4). Indeed, 86% of neurons exhibited their peak response at spatial phases within ± 45 deg of zero. A complete 'null' (PDI = 1.0) was exhibited by 36% of the neurons. The relationship between PDI and goodness-of-fit (R^2) values derived from fitting Equation 6 is shown in Figure 5*A*. Although in principle a relatively low R^2 could equally reflect either a weak phase-dependency or a jagged (noisy) but strong phase-dependence, there is a clear systematic trend

311 for low R^2 values to be associated with the low PDI values, suggesting it is predominantly a
312 characteristic of cells exhibiting little or no phase-selectivity.
313
314 Since the anesthesia changed between earlier and later experiments, we checked whether the
315 anesthesia type was predictive of the degree of phase sensitivity. For each anesthesia type,
316 the PDIs were distributed across the possible range. An independent samples t-test showed
317 that the PDIs did not differ significantly with the type of anesthesia (t = 1.76; df = 26; p =
318 0.0902). Therefore we do not believe the change in anesthesia had an effect on the degree of
319 phase sensitivity.
320
321 The preference of most neurons for a near-zero phase might suggest that this is a
322 consequence of visual neurons responding better to "dark" than to "light" stimuli (e.g. Yeh et
323 al, 2009; ~~Komban~~Jin et al, 20~~14~~08), since there is a perceptual appearance that the dark bars
324 of LM appear more prominent for the in-phase condition (Figure 1*E*, *F*). However in our
325 stimuli the luminance modulation (LM) was simply linearly added to the contrast modulation
326 (CM) - so both the light and dark bars/bands of the LM are always physically present, i.e. at
327 all relative spatial phases. From the 1-d profiles in Figure 1*G*,*H* it is clear that the net
328 excursions above and below the mean are equivalent for both the in-phase and anti-phase
329 stimuli.
330
331 Our electrode penetrations were slightly oblique to the surface, traversing all the laminae
332 down to white matter. However there was no systematic significant relationship between the
333 PDI value and depth of the recording (Pearson product-moment correlation r = -0.0248; df =
334 26; p = 0.9023). The neurons with the highest PDI values (1.0) spanned the full range of
335 recorded depths. Thus it is highly unlikely that the high PDI cells were concentrated

preferentially within a particular range of depths.

To quantify how a given neuron's summation of the two kinds of stimuli differs from simple linear additivity, and how this nonlinearity differs from one neuron to another, we also calculated the following ratios:

$$\textit{Enhancement ratio} = R_{max} / (R_{eq} - R_{spon}), \quad (8)$$

$$\textit{Suppression ratio} = R_{min} / (R_{eq} - R_{spon}), \quad (9)$$

where R_{eq} is the firing rate of the neuron that was chosen to equate the grating and envelope contrasts of the stimuli used to investigate phase interactions, and R_{spon} is the neuron's spontaneous firing rate. Note that R_{spon} is not removed in the numerators of these ratios, because R_{max} and R_{min} are obtained from curve-fits to spontaneous-subtracted responses. R_{eq}, however, is a measured response value, which includes the spontaneous rate. The R_{spon} values were measured from the average responses to the blank conditions that were interleaved with the phase conditions in the LM + CM experiment. These spontaneous rate values were not significantly different from those similarly obtained from the LM and CM contrast response measurements, as confirmed with a 1-way, repeated measures ANOVA ($F_{(2, 50)} = 1.335$; $p = 0.2724$).

One neuron was excluded from this analysis because the derived R_{spon} values marginally exceeded the R_{eq} values. An enhancement ratio of two (red dashed line, Fig. 5*B*) indicates that the maximal response (R_{max}) of the cell is exactly twice as much to both stimuli together as to each in isolation (linear summation). Similarly a suppression ratio of zero (blue dashed

line, Fig. 5*B*) indicates complete nulling of the neuron's response when the stimuli are in anti-phase (R_{min}), relative to ϕ_{max}. Enhancement ratios spanned 0.627 to 4.209 (mean = 2.082) and suppression ratios spanned 1.647 to -0.933 (mean = 0.342), indicating considerable heterogeneity amongst our neuron population (Fig. 5*B*). There was a moderate tendency for the magnitude of the suppression ratio to decrease as PDI increased, indicating a greater suppressive influence for neurons that exhibited the largest phase-dependencies. Whether neurons were simple- or complex-type did not systematically affect either ratio.

To confirm the appropriateness of our LM and CM response-matching procedure, for a number of neurons we measured phase-dependent interactions between LM and CM at two different response-matched contrasts. An example from a simple-type neuron is shown in Fig. 6. LM (Fig. 6*A*) and CM (Fig. 6*B*) contrasts were matched at either 14 (purple dotted lines) or 28 (green dotted lines) spikes/sec. Comparable phase-dependence was evident at both response-matched amplitudes (14 spikes/sec, Fig 6*C*; 28 spikes/sec, Fig. 6*D*), with similar ϕ_{max} and PDI values for each, thereby verifying the robustness of our matching paradigm and confirming that the absolute firing rate chosen to equate the two types of stimuli was not critical to the pattern of results found.

Some of the sampled neurons were simple-type cells, and thus had modulated responses to the drifting LM or CM stimuli. We wondered whether analysis of the temporal phases of these responses might be related to the dependence on relative phase of LM and CM stimuli. To do this we examined the temporal phase of the first harmonic at the equated contrast value, in the contrast response measurements (interpolating where necessary) for LM and CM gratings. Figure 7*A* shows that the amount of phase interaction, PDI, did not show a significant relationship with the difference in temporal phases for LM and CM responses (Pearson product moment correlation coefficient r = -0.4750; df = 6; p = 0.2342), though this

386 may not be surprising in view of the small sample size. However in Figure 7*B*, ϕ_{max} shows a
387 clear and statistically significant positive association (r = 0.9088; df = 6; p = 0.0018) with the
388 temporal phase difference. As the temporal phase difference increases, the ϕ_{max} also
389 systematically increases. So it looks like a lawful and expected relationship, for the simple
390 cells at least, that the variation in ϕ_{max} away from a relative spatial phase of zero is driven by
391 the difference in the temporal phases of the response to the two types of stimulus.
392
393 Amplitude-dependent responses
394 Neurons typically exhibited an enhanced response when LM and CM stimuli were phase-
395 aligned and a diminished response at or around anti-phase (Fig. 2*C*, Fig. 3 and Fig. 6*C*,*D*).
396 However the magnitude of the neuronal response might be not only determined by the spatial
397 phase offset between LM and CM — it could also be affected by other factors such as the
398 relative amplitudes of the two spatially superimposed stimuli. When LM and CM stimuli
399 were equated in terms of response, neurons produced a 'null' or minimum response at anti-
400 phase, compared to their 'in-phase' response. This is presumably because, in the former
401 condition, LM and CM effectively cancelled each other out (Fig. 1*F*) and no net driving
402 signal was available to the neuron. At anti-phase, effective visual information can be
403 reintroduced by increasing the amplitude of one stimulus relative to the other so that they are
404 no longer effectively balanced. If one stimulus drives the neuron more strongly than the
405 other, the nulling would be abolished and the neuron should become more responsive. To test
406 this notion, we fixed the amplitude of the CM stimulus at the value used to measure phase-
407 dependent interactions, and varied the contrast of the LM stimulus at the neuron's null-phase,
408 so that it was either less than, greater than, or equal to that derived from the response-
409 matching procedure (green arrows in Fig. 8). When stimuli were superimposed in anti-phase
410 with their amplitudes carefully equated, the neuron produced a minimal response. However

411 when the LM contrast was either reduced or increased beyond this match point, the neuron's
412 response increased as the two superimposed stimuli became progressively mismatched.
413 Figure 8*B-E* shows results from a further four representative neurons. The precise nature of
414 the interaction varied according to the contrast range employed in each neuron, which was
415 determined by the contrast response functions (CRFs) for each stimulus type and constrained
416 by the requirement that the sum of the LM grating contrast and CM carrier contrast cannot
417 exceed 100%. Among the examples of these measurements shown in Figure 8, some cells
418 exhibited responses that were reasonably symmetrical around the central match point (Fig.
419 8*A,B,D*), indicating that LM and CM were well equated at this contrast level. In some cases
420 the responses were appreciably less symmetrical, which may be due in part to imperfect
421 equating of the stimulus components (Fig. 8*C*) or the limited contrast range available (Fig.
422 8*E*).
423
424
425 **Discussion**
426
427 We have shown that neurons in early visual cortex, which respond form-cue invariantly to
428 first-order luminance gratings (LM) and second-order contrast envelopes (CM), responded in
429 a systematic manner to the relative spatial phase offset between the two kinds of patterns
430 when they are superimposed. In both simple- and complex-type cells, maximal responses
431 typically occurred when response-equated LM and CM were superimposed at or close to
432 phase-alignment, with a minimal response when in anti-phase. In many cases maximal and
433 minimal responses were markedly different, to varying degrees in different neurons. Neurons
434 varied substantially in the relative roles of suppressive or facilitative interaction effects. The
435 degree of this interaction between LM and CM at anti-phase could be modified by increasing

436 the amplitude of one stimulus relative to the other - when the LM amplitude was either
437 reduced or increased around a fixed CM amplitude, responses increased as the two
438 superimposed stimuli became progressively mismatched.
439
440 An important concern in experiments utilizing CM stimuli is that the observed neuronal
441 responses might be due to "distortion products" from nonlinearities of the display device or
442 the photoreceptors (Zhou & Baker, 1994; MacLeod et al., 1992). Such artifactual responses
443 would occur irrespective of carrier pattern characteristics. CM responses here were
444 selectively tuned to relatively high values of carrier spatial frequency, well outside the
445 luminance passband, and thus highly unlikely to be artifactual. The phase-dependence of the
446 response to combined LM and CM could arise in a similarly artifactual manner. However, in
447 that case the optimal phase value would always be the same - for example an early expansive
448 nonlinearity would always give $\phi_{max} = 0$ deg. This is because an expansive nonlinearity
449 introduces a distortion product into the neural representation of a contrast-modulated image,
450 with the same frequency and phase as the modulating waveform (see Figure 1 of Smith &
451 Ledgeway, 1997), that will combine with a superimposed luminance grating of the same
452 spatial phase to produce a maximal response. We observed a considerable scatter in values of
453 optimal phase in different neurons, again making such a possibility highly unlikely.
454
455 It is entirely possible that we may have missed some relevant neurons, due to our protocol.
456 Our neuron search stimulus was a bar of light and, as such, would not reveal neurons that
457 were responsive to only CM stimulus attributes, or even possibly a CM-driven neuron whose
458 response to CM can be modulated by LM. We only examined neurons that responded both to
459 LM and to CM in isolation, so we might have missed, for example, neurons that are
460 unresponsive to CM in isolation, but whose LM response is differentially affected by

461 superposition of CM stimuli in different relative phases. Moreover there might exist neurons
462 that respond only to specific stimulus combinations, but not to LM or CM stimuli alone.
463 Currently there is no evidence for the existence of neurons having such highly nonlinear
464 summation, but if they were present we would have missed them.
465
466 Psychophysical studies of LM and CM mixtures
467 Psychophysical studies have examined the degree to which first- and second-order cues
468 interact perceptually when they are spatially superimposed. Smith and Scott-Samuel (1998),
469 for example, showed that spatial frequency discrimination and speed discrimination could be
470 enhanced when first- and second-order gratings were superimposed compared to when each
471 was presented alone. Similarly Johnson et al. (2007) found that texture discrimination was
472 enhanced or impaired depending on whether the local elements comprising the textures
473 contained spatially correlated or uncorrelated LM and CM information respectively.
474
475 Masking studies have also investigated whether LM and CM gratings interact in a phase-
476 specific manner, the underlying assumption being that if the two types of stimuli are encoded
477 by a common mechanism, then detection should be highly dependent on the two patterns'
478 relative spatial phase. For example Badcock and Derrington (1989) explored the possibility
479 that second-order motion, defined by variations in contrast, is detected on the basis of a
480 distortion product, by adding a moving sine grating (LM) to a drifting beat (CM) pattern of
481 the same spatial frequency. The LM was 180 degrees out of phase with the CM and its
482 amplitude was varied in an attempt to null the hypothetical distortion product. They found
483 that direction-identification performance was unimpaired by the presence of the moving LM.
484 Lu and Sperling (1995) also found no appreciable phase-dependency when performance was
485 measured for combinations of drifting LM and CM noise matched for spatial frequency and

effective amplitude, although others (Scott-Samuel & Georgeson, 1999; Allard & Faubert, 2013) have reported phase-dependence but only at high temporal frequencies (15 Hz). Studies using stationary patterns are also equivocal with regard to the influence of relative spatial phase. Some have found moderate to strong phase-selectivity (e.g. Henning et al, 1975; Nachmias, 1989) whilst others have reported that masking magnitude is independent of phase (e.g. Cropper, 1998; Willis et al., 2000). A complication is that other factors such as extended practice, individual differences, local luminance cues in the image and the predictability of the phase relationships on each trial are also known to influence performance on this task (Nachmias & Rogowitz, 1983; Badcock, 1984). One possibility that could reconcile these discrepant results is that the human visual system contains neurons responsive to both LM and CM but with a range of phase selectivity (c.f. Fig. 3). Performance in a given situation could depend on which neurons are most sensitive, giving rise to either phase-independent or phase-specific masking.

Neural mechanisms

In early visual cortex of the cat and the macaque, a substantial fraction of the neurons respond both to first- and second-order patterns (Zhou & Baker, 1994; Li et al, 2014). Most proposed models of such responses involve two parallel signal processing pathways, each specialized for one or the other type of stimulus, whose signals are then combined (Mareschal & Baker, 1999). Alternatively, cortical second-order responses could originate from LGN (and ultimately retinal) Y-cells, whose responses carry both luminance information at low spatial frequencies and specificity for carrier attributes at high frequencies (Rosenberg & Issa, 2011). The present findings of phase-dependent combination are not incompatible with either of these schemes. Models based on human psychophysics have involved separate early detection of the two kinds of stimuli, with subsequent interactions at a later stage (Georgeson

& Schofield, 2002). A model with cross-wise gain control interactions between pathways carrying a mixture of first-and second-order information (Schofield et al, 2010; Sun & Schofield, 2011) predicts our observations of stronger responses to in-phase than anti-phase conditions.

As a baseline reference, it is worth considering that a cortical neuron might just linearly add the separately computed responses to LM and CM stimuli. In the case of a simple-type cell, the modulated responses to the LM and CM stimuli would sum maximally at one phase, and cancel out at the opposite phase, giving a PDI approaching unity. In fact the optimal relative phase values were linearly predictable from the phase lags of the LM and CM alone (Fig. 7B). The lack of relationship to the PDI value (Fig. 7A) may be because the effect of the temporal phase lag is to effectively shift the ϕ_{max} value in a neuron which already is, or is not, phase-selective. Complex-type cells might be thought of as linearly adding energy-like responses to LM and CM stimuli, which would not be modulated, and hence their summation should be phase-invariant (PDI about zero). Alternatively a complex cell might result from an energy-type operation on pooled responses of simple cell (modulated) responses to LM and CM stimuli, whose early summation would give a high PDI. In our sample the complex-type cells showed a wide range of PDI values (Fig. 4), suggesting a continuum between such types of models.

Functional implications / Significance

These neurons show complex interactions between both amplitude and phase of LM and CM components, which are in some cases consistent with vector summation. This finding suggests a modification of the form-cue invariance principle (Albright, 1992) - while these neurons are form-cue invariant to orientation, spatial frequency, and motion direction, they

536 are in most cases not invariant to the relative phase of superimposed first- and second-order
537 components.
538
539 These properties might have implications for how the visual system processes natural images.
540 Neurons with little or no LM + CM phase-dependence would respond to boundaries
541 regardless of the configuration of their components, while those having a strong phase
542 dependency would respond selectively to particular co-occurrences of first- and second-order
543 information in natural images (Johnson & Baker, 2004). These neurons' responses carry
544 information that may help disambiguate whether luminance changes in the retinal image arise
545 from surface reflectance changes, or from illumination gradients such as shading or shadows
546 (Schofield et al, 2006; 2010; Sun and Schofield, 2011). More generally, the heterogeneity in
547 degree of phase-dependent interactions and suppression vs. enhancement might provide a
548 basis for disambiguating or decoding a variety of different kinds of boundaries. A promising
549 future direction would be to examine the relative phases of LM and CM components at
550 boundaries in natural images that arise from different causes.
551

552 **References**

553

554 Albright TD (1992) Form-cue invariant motion processing in primate visual cortex. Science
555 255:1141-1143.

556

557 Allard R, Faubert J (2013) No second-order motion system sensitive to high temporal
558 frequencies. Journal of Vision 13(5):4, 1–14, http://www.journalofvision.org/content/13/5/4,
559 doi:10.1167/13.5.4.

560

561 Badcock DR (1984) Spatial phase or luminance profile discrimination. Vision Research
562 24:613-623.

563

564 Badcock DR, Derrington AM (1989) Detecting the displacement of spatial beats: no role for
565 distortion products. Vision Research 29:731-739.

566

567 Brainard DH (1997) The psychophysics toolbox. Spatial Vision 10:433-436.

568

569 Chaudhuri A, Albright TD (1997) Neuronal responses to edges defined by luminance vs.
570 temporal texture in macaque area V1. Visual Neuroscience 14:949-962.

571

572 Cropper SJ (1998) Detection of chromatic and luminance contrast modulation by the visual
573 system. Journal of the Optical Society of America A 15:1969-1986.

574

575 Efron B, Tibshirani RJ (1993) An Introduction to the Bootstrap. London: Chapman & Hall.

576

El-Shamayleh Y, Movshon JA (2011) Neuronal responses to texture-defined form in macaque visual area V2. J Neuroscience 31:8543-8555.

Geesaman BJ, Anderson RA (1996) The analysis of complex motion patterns by form/cue invariant MSTd neurons. Journal of Neurophysiology 16:4716-4732.

Georgeson MA, Schofield, AJ (2002) Shading and texture: Separate information channels with a common adaptation mechanism? Spatial Vision 16:59-76.

Hallum LE, Landy MS, Heeger, DJ (2011) Human primary visual cortex is selective for second-order spatial frequency. Journal of Neurophysiology 105:2121-2131.

Henning GB, Hertz BG, Broadbent DE (1975) Some experiments bearing on the hypothesis that the visual system analyzes patterns in independent bands of spatial frequency. Vision Research 15:887-899.

Jin JZ, Weng C, Yeh C-I, Gordon JA, Ruthazer ES, Stryker MP, Swadlow HA, Alonso J-M. (2008) On and off domains of geniculate afferents in cat primary visual cortex. Nature Neuroscience 11:88-94.

Johnson AP, Baker CL (2004) First- and second-order information in natural images: A filter-based approach to image statistics. Journal of the Optical Society of America A 21:913-925.

601 Johnson AP, Prins N, Kingdom FA, Baker CL Jr. (2007) Ecologically valid combinations of
602 first- and second-order surface markings facilitate texture discrimination. Vision Research
603 47:2281-90.
604
605 Kleiner M, Brainard D, Pelli D (2007) What's new in Psychtoolbox-3? In: Paper presented at
606 the 36th European Conference on Visual Perception. Arezzo, Italy.
607
608 ~~Komban SJ, Kremkow J, Jin J, Wang Y, Lashgari R, Li X, Zaidi Q, Alonso J-M (2014)~~
609 ~~Neuronal and perceptual differences in the temporal processing of darks and lights. Neuron~~
610 ~~82(1): 224-234.~~
611
612 Larsson J, Landy MS, Heeger DJ (2006) Orientation-selective adaptation to first- and second-
613 order patterns in human visual cortex. Journal of Neurophysiology 95:862–881.
614
615 Ledgeway T, Zhan C, Johnson AP, Song Y, Baker, CL Jr. (2005) The direction selective
616 contrast response of area 18 neurons is different for first- and second-order motion. Visual
617 Neuroscience 22:87-99.
618
619 Li G, Yao Z, Wang Z, Yuan N, Talebi V, Tan J, Wang Y, Zhou Y, Baker CL Jr. (2014)
620 Form-cue invariant second-order neuronal responses to contrast modulation in primate area
621 V2. J Neuroscience 34:12081-12092.
622
623 Lu Z-L, Sperling G (1995) The functional architecture of human visual motion perception.
624 Vision Research 35:2697-2722.
625

626 MacLeod DI, Williams DR, Makous W (1992) A visual nonlinearity fed by single cones.
627 Vision Res 32:347-363.
628
629 Mareschal I, Baker CL Jr. (1999) Cortical processing of second-order motion. Visual
630 Neuroscience 16:1-14.
631
632 Nachmias J (1989) Contrast modulated maskers: test of a late nonlinearity hypothesis. Vision
633 Research 29:137-142.
634
635 Nachmias J, Rogowitz BE (1983) Masking by spatially modulated gratings. Vision Research
636 23:1621-1630.
637
638 Nishida S, Sasaki Y, Murakami I, Watanabe T, Tootell RBH (2003) Neuroimaging of
639 direction-selective mechanisms for second-order motion. Journal of Neurophysiology
640 90:3242-3254.
641
642 Pelli DG (1997). The VideoToolbox software for visual psychophysics: transforming
643 numbers into movies. Spatial Vision, 10(4), 437-442.
644
645 Rosenberg A, Issa NP (2011) The Y cell visual pathway implements a demodulating
646 nonlinearity. Neuron 71:348-361.
647
648 Schofield AJ (2000) What does second-order vision see in an image ? Perception 29:1071-
649 1086.
650

651 Schofield AJ, Hesse G, Rock PB, Georgeson MA (2006) Local luminance amplitude
652 modulates the interpretation of shape-from-shading in textured surfaces. Vision Research,
653 46:3462-3482.
654
655 Schofield AJ, Rock PB, Sun P, Jiang X, Georgeson MA (2010) What is second-order vision
656 for? Discriminating illumination versus material changes, Journal of Vision 10(9): 2;
657 doi:10.1167/10.9.2.
658
659 Scott-Samuel NE, Georgeson MA (1999) Does early non-linearity account for second-order
660 motion? Vision Research 39:2853-2865.
661
662 Seiffert AE, Somers DC, Dale AM, Tootell RBH (2003) Functional MRI studies of human
663 visual motion perception: texture, luminance, attention and after-effects. Cerebral Cortex 13:
664 340-349.
665
666 Skottun BC, De Valois RL, Grosof D, Movshon JA, Albrecht DG, Bonds AB (1991)
667 Classifying simple and complex cells on the basis of response modulation. Vision Research
668 31:1079–1086.
669
670 Smith AT, Ledgeway T (1997) Separate detection of moving luminance and contrast
671 modulations: Fact or artifact. Vision Research 37:45–62.
672
673 Smith AT, Scott-Samuel NE (1998) Stereoscopic and contrast-defined motion in human
674 vision. Proceedings of the Royal Society of London B. 265:1573-1581.
675

676 Sun P, Schofield AJ (2011) The efficacy of local luminance amplitude in disambiguating the
677 origin of luminance signals depends on carrier frequency: Further evidence for the active
678 role of second-order vision in layer decomposition. Vision Research 51:496-507.
679
680 Tanaka, H., & Ohzawa, I. (2006). Neural basis for stereopsis from second-order contrast
681 cues. J. Neurosci. 26:4370-4382.
682
683 Tusa RJ, Rosenquist AC, Palmer LA (1979) Retinotopic organization of area 18 and 19 in the
684 cat. J Comp Neurol 185:657-678.
685
686 Willis A, Smallman HS, Harris JM (2000) Comparing contrast-modulated and luminance-
687 modulated masking: effects of spatial frequency and phase. Perception 29:81-100.
688
689 Yeh C-I, Xing D, Shapley RM (2009) "Black" responses dominate macaque primary visual
690 cortex V1. J Neurosci 29(38) 11753-60.
691
692 Zhou YX, Baker CL Jr. (1994) Envelope-responsive neurons in area 17 and 18 of cat. Journal
693 of Neurophysiology 72:2134-2150.
694
695
696

Figure legends

Figure 1. Examples of stimulus composition for main experiment~~.~~, in which one luminance grating (LM) phase is combined with two different contrast envelope (CM) phases. ***A***, Luminance grating (LM) added to ~~*C*~~***B***, contrast envelope (CM) of the same spatial phase produced ~~***E***~~***C***, an in-phase (0 deg offset) composite stimulus~~.~~ - note that only the contrast variations about the mean background were added, as detailed in Equation 5. Luminance and contrast modulations (LM & CM) were taken to be in-phase~~-aligned~~ when high and low luminance and high and low contrast bars of the grating and envelope, respectively, were phase-aligned. ~~***B,***~~***D,*** 1-d luminance profile corresponding to stimulus image in *C*. ***E,F,G,H,*** same as *A,B,C,*~~*E*~~*D* but the component patterns were summed in anti-phase (180 deg relative phase offset) producing a composite stimulus ~~(***F***)~~*G* in which the high and low luminance bars of the grating were centered on the low and high contrast bars of the envelope, respectively. ~~***G,H***, 1-d luminance profiles corresponding to stimulus images in *E,F* respectively~~ See text for further details.

Figure 2. Contrast response functions (CRFs) and phase-dependent interaction, for LM and CM stimuli whose parameters are optimized for an example complex-type cell. ***A***,***B***, CRFs for a luminance grating and an envelope, respectively. Error bars represent ± 1 S.E.M. Dashed red lines represent spontaneous activity (responses to a blank field). Dashed green lines show the grating (LM) contrast and envelope (CM) contrast that elicited an equivalent average spike frequency from the neuron. These response-matched contrasts were used to superimpose the grating and envelope at a series of relative phase offsets (0-330 deg). Both components of the composite stimuli moved together in the neuron's preferred direction. ***C***, Average spike frequencies as a function of relative phase offset of the composite stimuli.

Dashed black lines represent ± 1 S.E.M. The red line indicates spontaneous activity. This neuron exhibited responses that depended upon the relative phase relationship between LM and CM stimuli, with maximal response when they were superimposed approximately 'in phase' and minimal response when close to 'anti-phase'. These data were well fit (solid blue line) by a descriptive function (Equation 6), used to derive a phase-dependency index (PDI, Equation 7) and an estimate of the phase offset (ϕ_{max}) that produced maximal responses.

Figure 3. Phase-dependent interactions for 6 representative neurons. Average spike frequency is plotted as a function of the spatial phase offset between response-equated LM and CM stimuli. Dashed black lines indicate ± 1 S.E.M. Dashed red lines show spontaneous activity. Data from each neuron have been fit (solid blue lines) with a descriptive function (Equation 6). Data from simple-type (***B,E***) and complex-type (***A,C,D,F***) cells are shown. Neurons displayed varying amounts of phase-dependent interaction. Phase offsets (ϕ_{max}) corresponding to maximal responses and phase-dependency indices (PDI) are shown at the top right of each polar plot.

Figure 4. Phase-dependent indices (PDI) plotted against optimal phase alignments (ϕ_{max}) for all neurons in the sample (N = 28). Simple-type neurons are denoted by red circles and complex-type by blue triangles. Marginal histograms show the distribution of ϕ_{max} (top) and PDI (right) values within the sample population. ϕ_{max} ranged from -103.42 to 107.35, with a mean of 6.57 deg. PDI values ranged from 0.09 to 1.0, with a mean of 0.71, indicating a wide range of relative phase dependencies in different neurons.

Figure 5. Goodness-of-fit and summation ratios for phase-dependent interactions. **A**, R^2 values derived from fitting Equation 6 to each neuron's responses to the combined LM and

CM patterns, plotted against the corresponding PDI values. Equation 6 best fit responses of neurons that exhibited a high degree of interaction with a well-defined null phase (PDI values ~ unity). ***B***, Enhancement and suppression ratios (Equations 8 and 9, respectively), indicating neurons' responses to LM and CM stimuli in isolation compared to responses to their composite at ϕ_{max} (enhancement ratio, red triangles) and ϕ_{max} - 180 deg (suppression ratio, blue triangles). An enhancement ratio of two (red dashed line) indicates R_{max} of the cell is exactly twice as much to both stimuli together as to each in isolation (linear summation). A suppression ratio of zero (blue dashed line) indicates complete nulling of the neuron's response at R_{min}. Different neurons exhibited a range of enhancement and suppression ratios, not always consistent with simple linear summation. Error bars around each of these ratios represent 68% confidence intervals (~ equivalent to ± 1 standard error) generated by a nonparametric, bias corrected and accelerated (BCa) bootstrapping technique that created 10,000 bootstrapped replications of each fitted function, without assuming a Gaussian distribution for the raw data or the residuals (Efron & Tibshirani, 1993).

Figure 6. CRFs and phase-dependent interactions at two different response-matched contrasts for a simple-type neuron. ***A***,***B***, CRFs for a luminance grating (LM) and a contrast envelope (CM), respectively. Error bars denote ± 1 S.E.M. Dashed red lines represent spontaneous activity. Dashed purple and green lines show the stimulus contrasts evoking equivalent responses from the neuron at two different spike frequencies (14 and 28 spikes/sec, respectively). ***C***, Phase-dependent interaction plot for component stimuli matched at 14 spikes/sec. ***D***, Same as ***C***, but for response-matching at 28 spikes/sec. In ***C*** and ***D*** dashed black lines above and below the data points represent ± 1 S.E.M. The red line shows spontaneous activity. Data were well fit by a descriptive function (Equation 6, solid blue line), which produced qualitatively and quantitatively similar results irrespective of the

absolute firing rate chosen to equate the two types of stimuli. Note that the derived ϕ_{max} and PDI values are almost identical (ϕ_{max} values were 40.01 deg and 40.65 deg and PDIs were 0.37 and 0.39) in each case.

Figure 7. Relationship of LM + CM phase interactions to temporal phase lags of responses in simple-type cells. ***A***, Amount of phase-dependent interaction (PDI) as a function of difference in temporal phase lag, measured for LM and for CM stimuli presented alone, in simple-type cells having modulated discharges. ***B***, Same as *A*, but optimal phase (ϕ_{max}) for response to LM + CM compound stimuli, showing an approximately linear relationship.

Figure 8. Contrast dependent interactions for 5 representative neurons. Data from simple-type (***D***) and complex-type (***A,B,C,E***) neurons are shown. A luminance grating (LM) and a contrast envelope (CM) were superimposed at the phase offset that produced the minimal response (**A**:210 deg, **B**:180 deg, **C**:150 deg, **D**:120 deg, **E**:180 deg) and their relative amplitudes (contrasts) varied. An example stimulus set is shown in **A**. Envelope (CM) contrast was fixed (100%), and grating (LM) contrast varied above and below the response-matched value. Red dashed lines show spontaneous activity. Green arrows show response-matched grating contrasts. Error bars represent ± 1 S.E.M. In most cases examined, firing rates increased as the two superimposed stimuli became progressively mismatched.

Figure 1

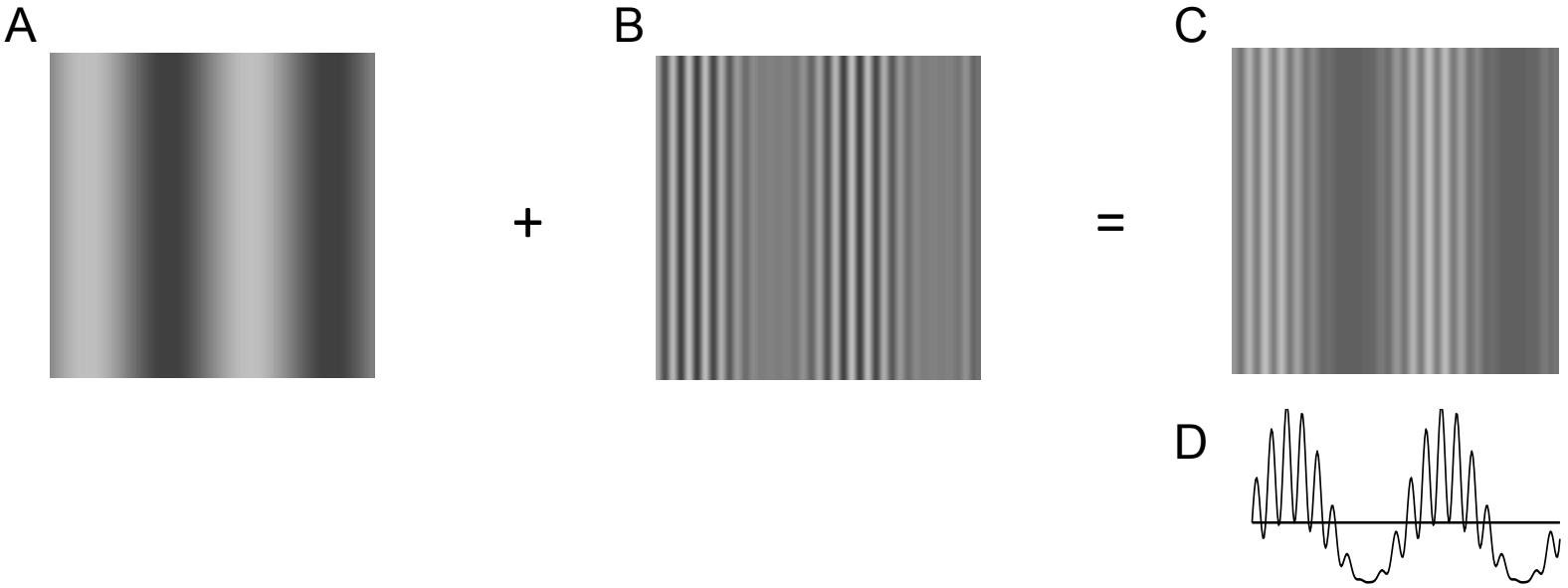

Figure 2

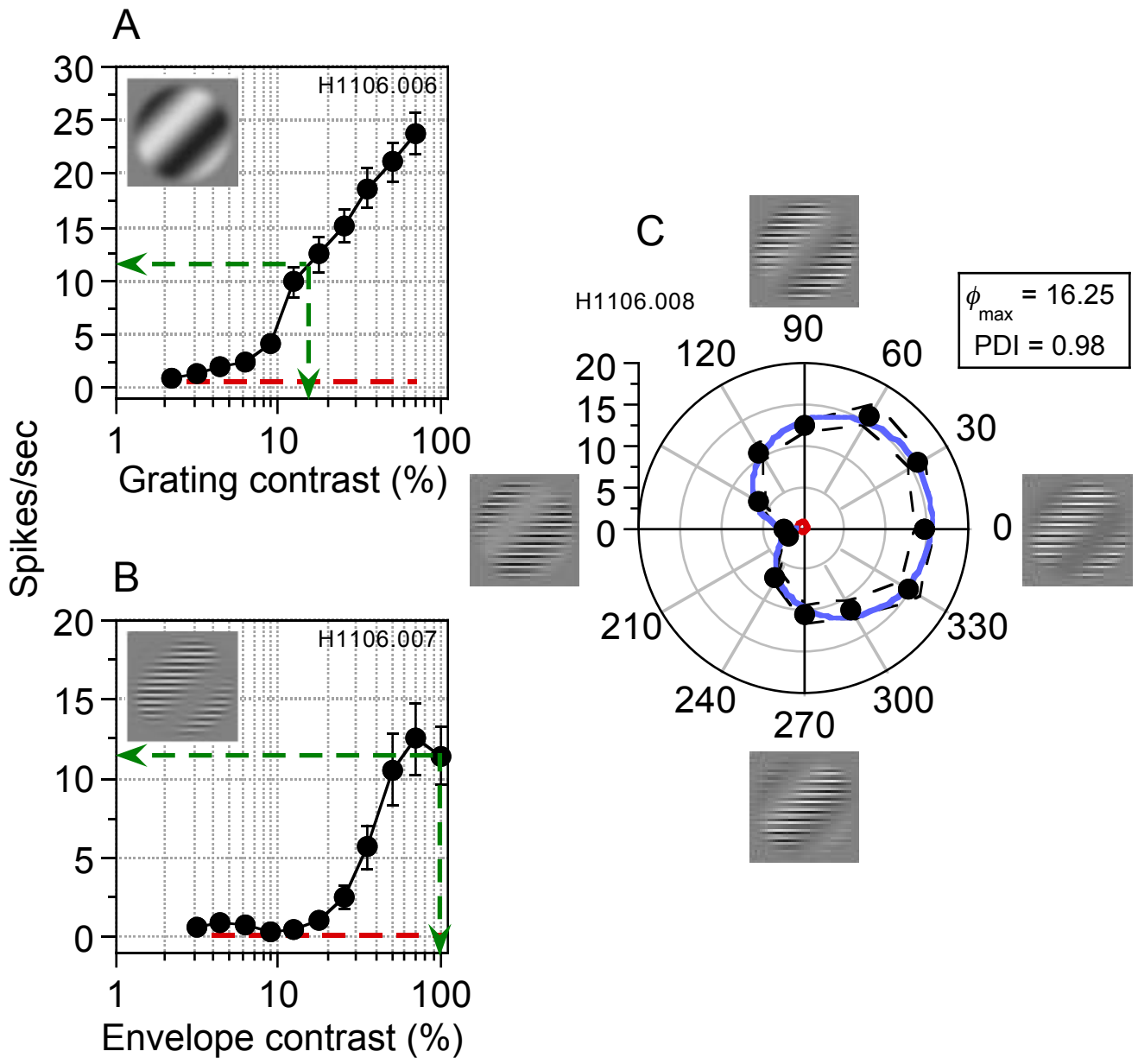
A
H1106.006
Spikes/sec
Grating contrast (%)
B
H1106.007
Envelope contrast (%)
C
H1106.008
ϕ_{max} = 16.25
PDI = 0.98
90
120
60
30
0
210
330
240
300
270

Figure 3

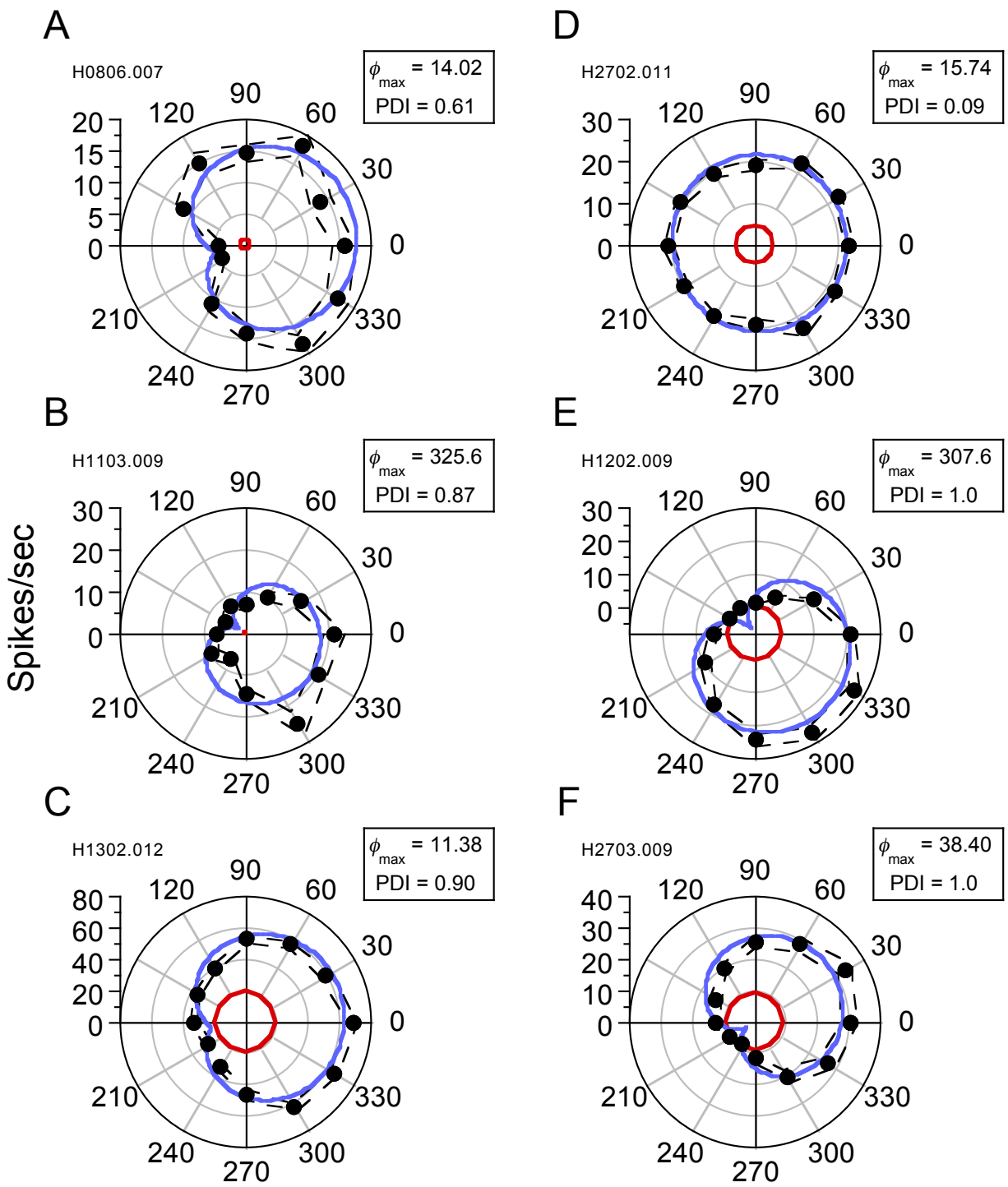
A
H0806.007
ϕ_{max} = 14.02
PDI = 0.61
B
H1103.009
ϕ_{max} = 325.6
PDI = 0.87
C
H1302.012
ϕ_{max} = 11.38
PDI = 0.90
D
H2702.011
ϕ_{max} = 15.74
PDI = 0.09
E
H1202.009
ϕ_{max} = 307.6
PDI = 1.0
F
H2703.009
ϕ_{max} = 38.40
PDI = 1.0
Spikes/sec
90
120
60
30
0
210
240
270
300
330

Figure 4

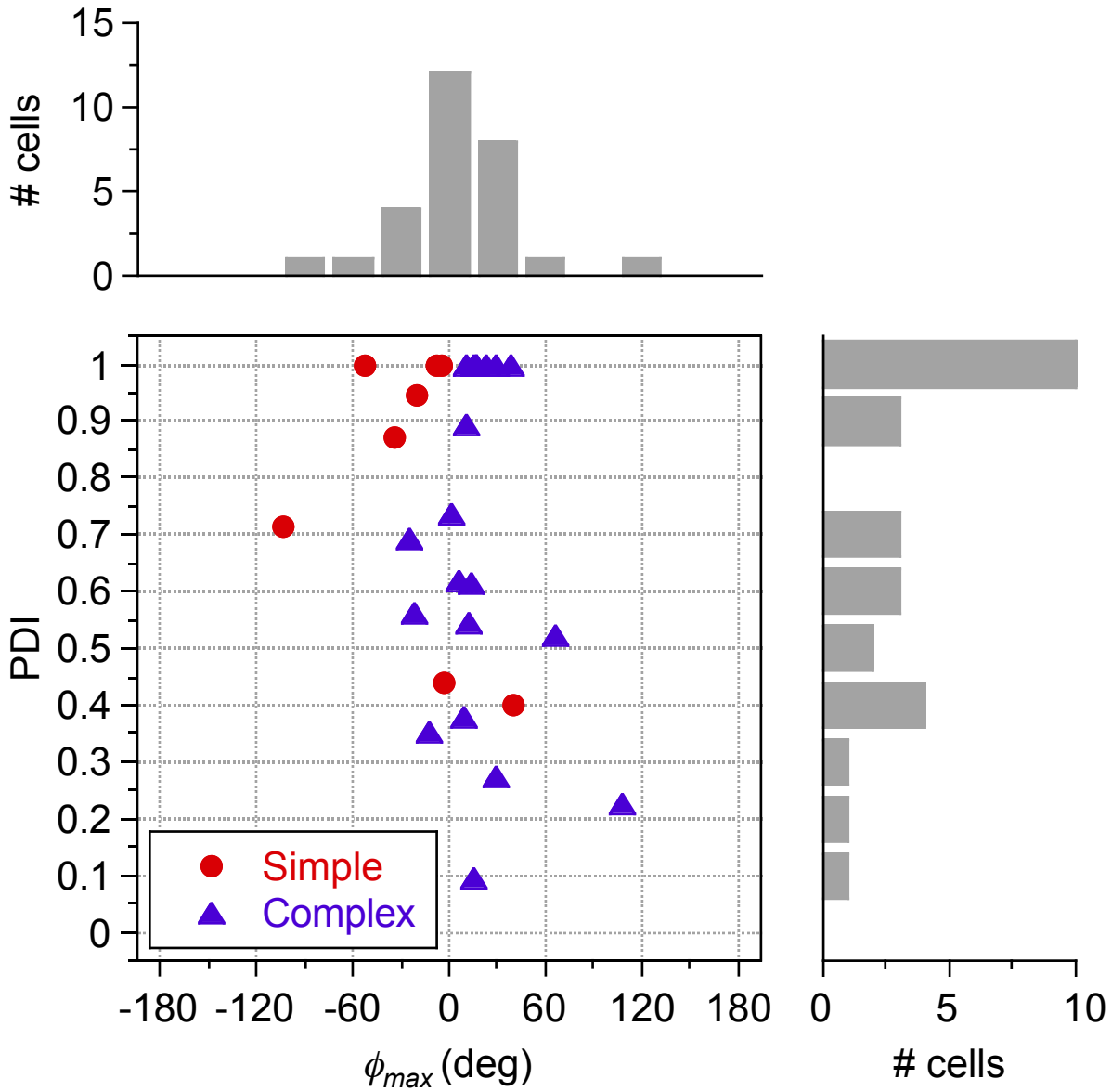
15
10
5
0
cells
1
0.9
0.8
0.7
0.6
0.5
0.4
0.3
0.2
0.1
0
PDI
Simple
Complex
-180
-120
-60
0
60
120
180
ϕ_{max} (deg)
0
5
10
cells

Figure 5

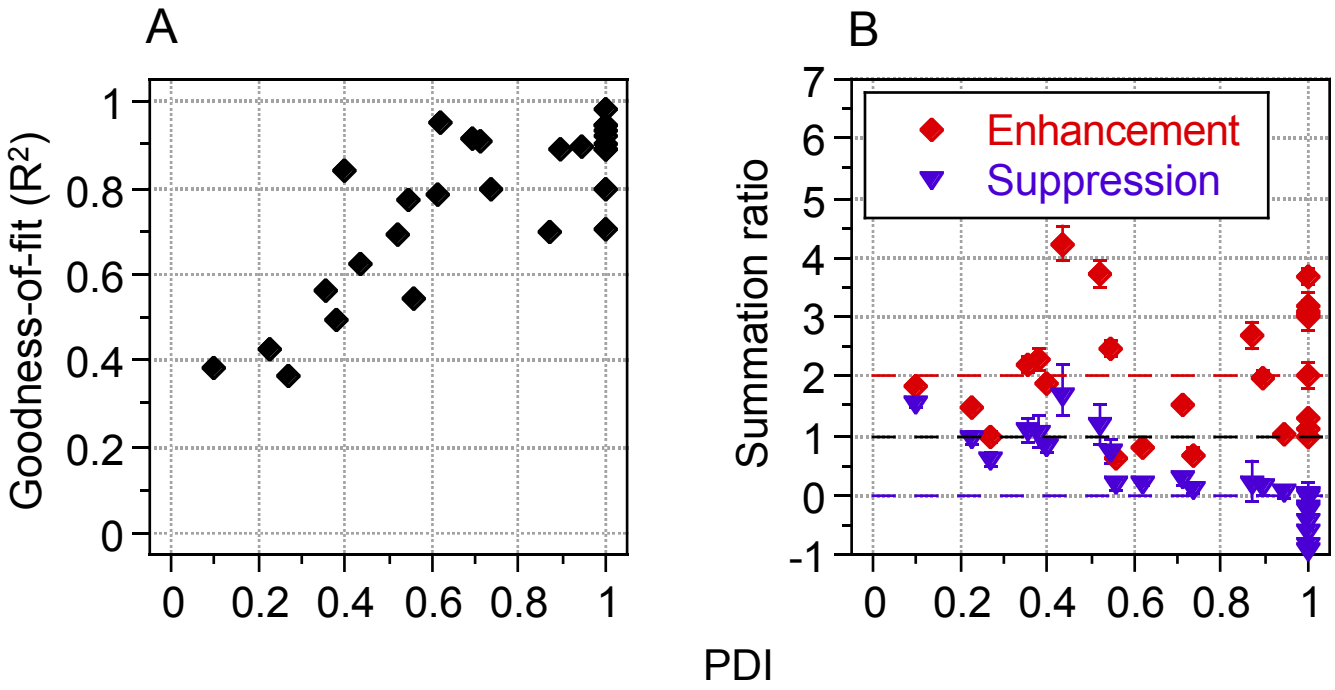
A
B
Goodness-of-fit (R^2)
Summation ratio
PDI
Enhancement
Suppression
0
0.2
0.4
0.6
0.8
1
-1
2
3
4
5
6
7

Figure 6

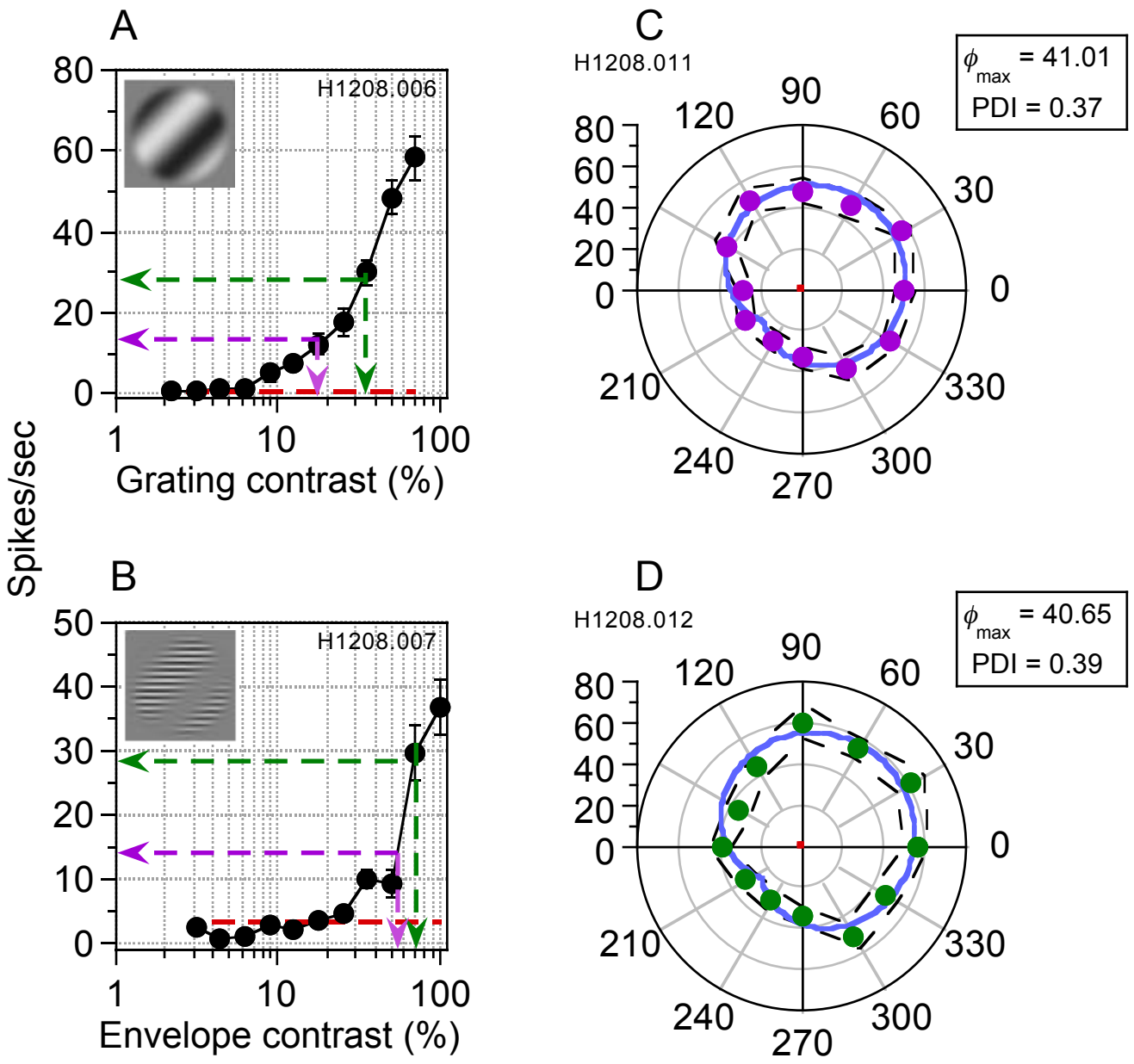
A
H1208.006
Spikes/sec
Grating contrast (%)
B
H1208.007
Envelope contrast (%)
C
H1208.011
ϕ_{max} = 41.01
PDI = 0.37
D
H1208.012
ϕ_{max} = 40.65
PDI = 0.39

Figure 7

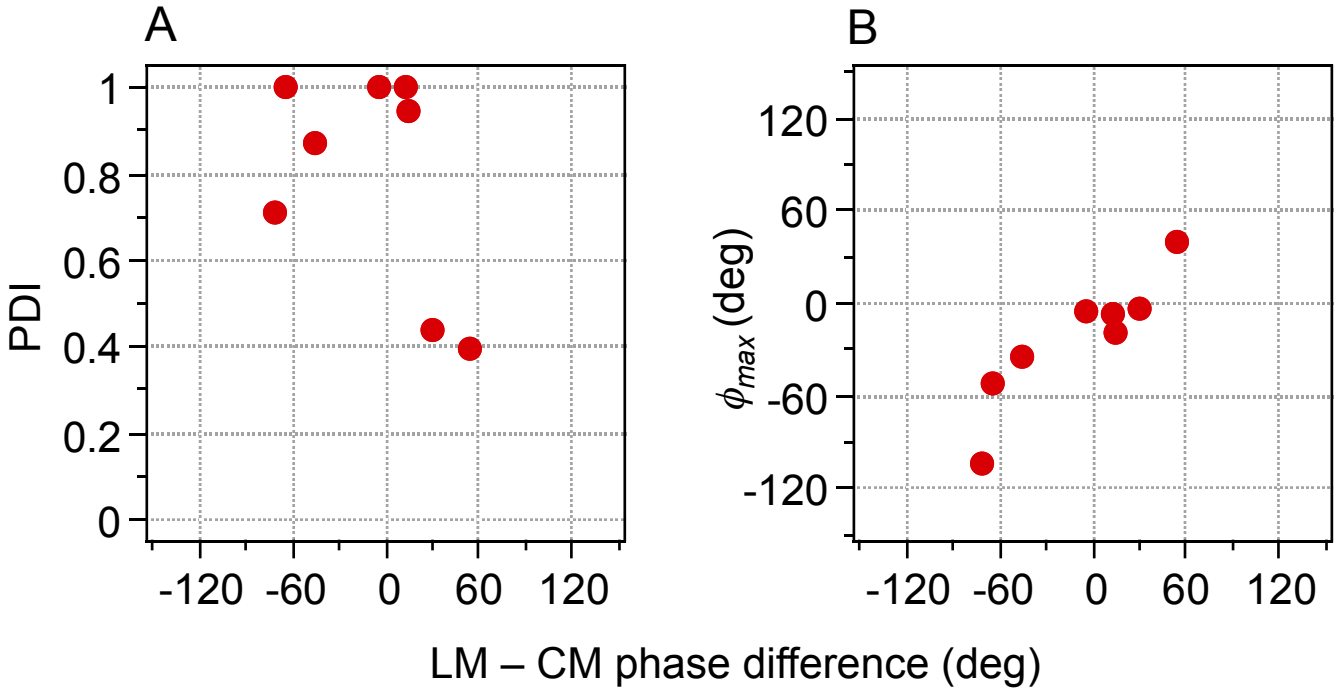
A
B
PDI
1
0.8
0.6
0.4
0.2
0
-120
-60
0
60
120
ϕ_{max} (deg)
120
60
0
-60
-120
LM – CM phase difference (deg)

Figure 8

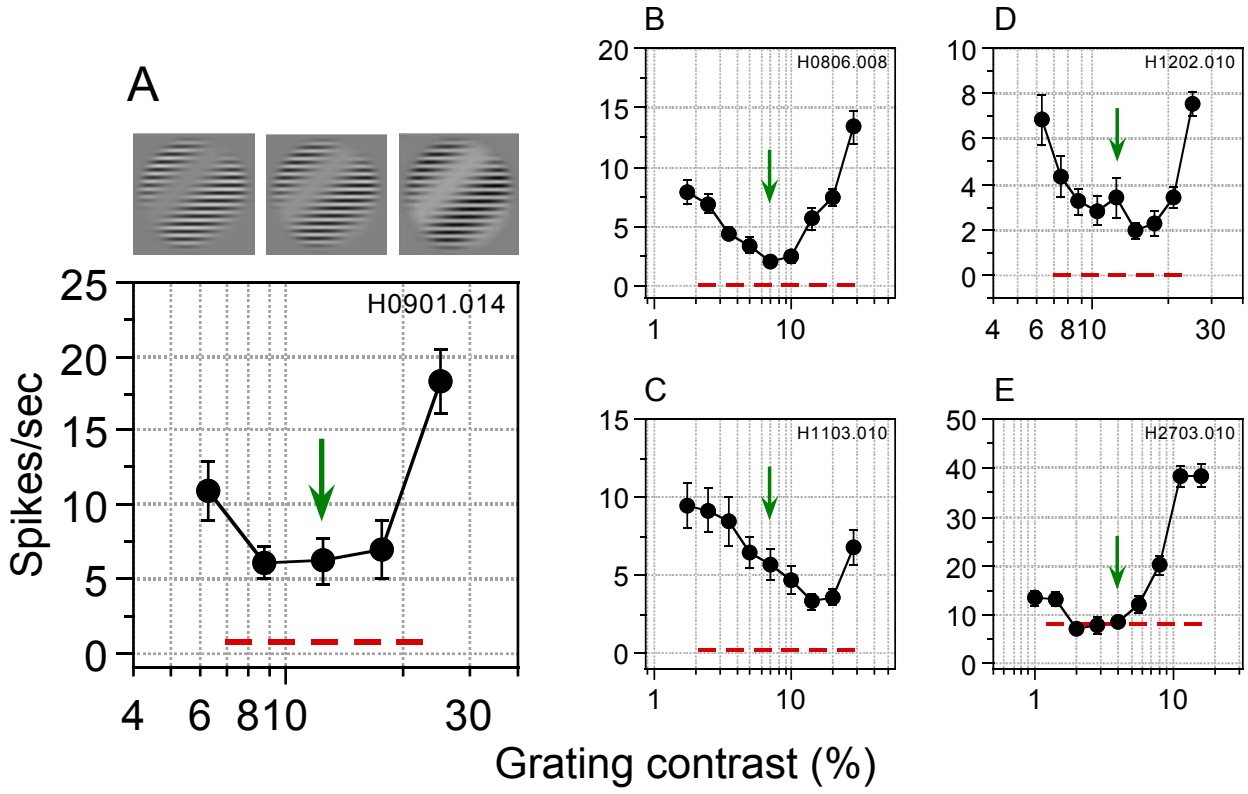
A
B
C
D
E
H0901.014
H0806.008
H1103.010
H1202.010
H2703.010
Spikes/sec
Grating contrast (%)